Reconstruction of heat flux profile on the HL-2A divertor plate with a three-dimensional analysis model*

Gao Jin-Ming(高金明)†, Li Wei(李 伟), Xia Zhi-Wei(夏志伟), Pan Yu-Dong(潘宇东), Lu Jie(卢 杰), Yi Ping(易 萍), and Liu Yi(刘 仪)

Southwestern Institute of Physics, Chengdu 610041, *China*

(Received 23 April 2012; revised manuscript received 19 June 2012)

A three-dimensional analysis model based on the finite element method (FEM) is developed, which can derive the evolution and distribution characteristics of heat flux deposited on the divertor plate from the surface temperature measured by infrared thermography diagnostics. The numerical simulations of surface heating due to localized power bursts and the power deposition calculations demonstrate that this analysis can provide accurate results and useful information about localized hot spots compared with the normal one- and two-dimensional calculations. In this paper, the details of this three-dimensional analysis are presented, and some results in ohmic heating and electron cyclotron resonant heating (ECRH) discharge on HL-2A are given.

Keywords: three-dimensional analysis, heat flux, divertor plate

PACS: 52.55.Fa, 52.55.Rk, 52.40.Hf **DOI:** 10.1088/1674-1056/22/1/015202

1. Introduction

In a divertor tokamak, a considerable part of the energy flux is deposited onto the target plates.[1,2] Since this power deposition may occur non-uniformly and instantaneously in small areas,[3–5] the erosion problem of divertor plates will become severe in reactor-relevant tokamak with high plasma power density and long discharge duration.[6] In order to optimize the design of components exposed to high heat fluxes, a detailed understanding of the heat flux pattern is necessary. Specifically, the power peak and width, the important characteristics of heat flux on the plate, have a close relation with the upstream conditions,[6] so the accurate calculation of the heat flux evolution is significant for the analysis of particle or heat transport.

Infrared (IR) thermography is a valuable tool to measure the evolution of the target surface temperature. And the heat flux can be routinely derived with space and time dependent surface temperature values by solving the heat diffusion equations numerically.[1,7] As the three-dimensional (3D) nonlinear analysis is very complicated, one- and two-dimensional (1D and 2D) heat diffusion equations are normally used to simplify the calculation, in which heat fluxes deposited on a target plate symmetrically along the toroidal direction are assumed.[1,7–9] However, the 3D analysis has been used to determine the thermal properties of carbon layer on carbon fibre composite (CFC) tiles because of erosion, transport, and redeposition of the carbon on JET.[10] And the results show its advantage of calculating the heat flux compared with the 1D analysis method. On HL-2A tokamak, the non-toroidal-symmetric strike points can be observed clearly in some discharges as shown in Fig. 1. For such hot spots, the 1D or 2D analysis of the actually 3D problem can lead to systematic misinterpretations, so a more accurate analysis method considering the 3D heat conduction in the plate is developed to use in such a case. The ANSYS is a universal finite element modeling package for numerically solving a wide variety of mechanical problems, which include heat transfer problems. Therefore, in the 3D analysis method, the ANSYS is applied to solving the non-stationary heat conduction equation for realizing an automated determination of the heat flux.

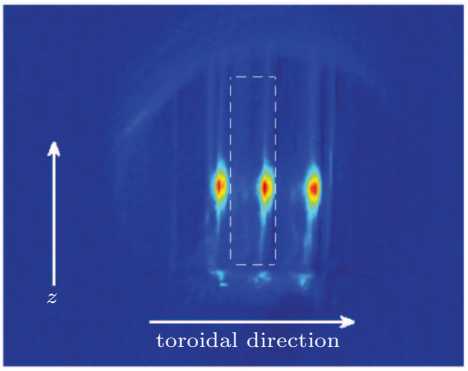

Fig. 1. (color online) Typical image captured by using an IR camera. The dashed line box is used as the work area for analysing heat flux onto the target plate.

In the rest of this paper, the thermographic diagnostic is introduced in Section 2. The details of a 3D model and analysis are presented in Section 3. The heat flux testing numerical data is shown in Section 4. Some experimental results using

*Project supported by the National Natural Science Foundation of China (Grant No. 10805016) and the National Magnetic Confinement Fusion Science Program, China (Grant No. 2009GB104008).

†Corresponding author. E-mail: gaojm@swip.ac.cn

© 2013 Chinese Physical Society and IOP Publishing Ltd

such an analysis are shown in Section 5. The conclusions are given in Section 6.

2. Experimental set-up

The HL-2A tokamak (with major radius $R = 1.65$ m and minor radius $a = 0.4$ m) has a close sysmmetric double-null divertor.[8] And the lower single null (LSN) divertor configuration is used in the recent experiment.

An IR camera system has been developed to measure the evolution of surface temperature on the outer divertor plates on HL-2A.[8] The current arrangement of IR camera system is shown schematically in Fig. 2. The IR camera with a Stirling cooler and an GaAs detector sensitive to the 8 μm-to-9 μm radiation can measure the surface temperature ranging from −20 °C to 2000 °C. A zinc selenide (ZnSe) window is coated for achieving a flat IR transmission of greater than 95% in the wavelength range of 6–14 μm. The frame rate is available from 60 Hz with a full frame of 320×240 camera pixels to 900 Hz with a frame of 320×16 pixels. The camera is equipped with a telephoto lens with a field of view of $9° \times 7°$, which can provide good coverage of the strike point on the outer divertor plates and a high spatial resolution of about 0.8 mm in the vertical direction. The surface temperature is corrected by object parameters and calibrated *in situ* in the temperature range from 20 °C to 120 °C during the baking period of HL-2A.

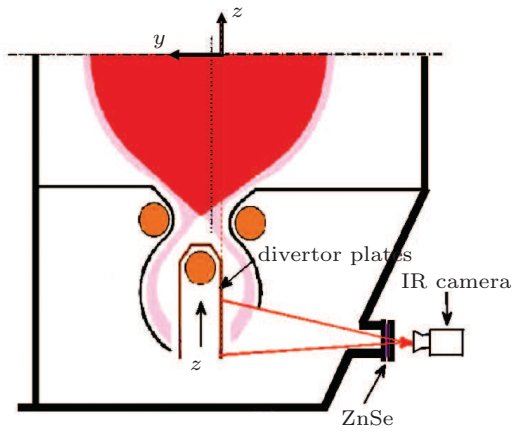

Fig. 2. (color online) Schematic arrangement of the IR camera system on HL-2A.

In addition, the plasma radiations in both the main chamber and the divertor chamber are monitored by four 16-channel pinhole type absolute extreme ultraviolet (AXUV) bolometer cameras.[11]

3. The 3D model for calculation of the deposited heat flux

In order to solve the problem of hot spot mentioned above, the 3D heat conduction in the plate must be considered, so a 3D geometric model is needed. On HL-2A, the geometric structure of the divertor plates is ribs-like with an elliptic water cooled loop inside. The material of plate is copper, of which the thermophysical parameters are shown in Table 1. The value of thermal conductivity is set according to the present experimental conditions. A 3D geometric model is reconstructed according to the real geometric structure of divertor plate, as shown in Fig. 3. The mesh length in the model is about 0.8 mm, which is much smaller than the typical full width at half maximum (FWHM) of the power deposition profile.

Table 1. Thermophysical parameters of the plate material.

	Copper
Thermal conductivity/$\mathrm{W \cdot m^{-1} \cdot K^{-1}}$	395
Density/$\mathrm{kg \cdot m^{-3}}$	8930
Specific heat/$\mathrm{J \cdot kg^{-1} \cdot K^{-1}}$	430
Thermal diffusivity/$\mathrm{m^2 \cdot s^{-1}}$	1.0287×10^{-4}

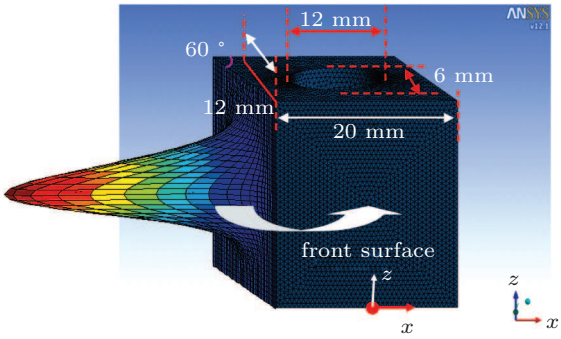

Fig. 3. (color online) The 3D geometric model of the divertor plate and the Gaussian distribution plot. The red dot represents the origin of the Cartesian coordinate in the simulation.

The heat flux on the divertor plates is computed from the spatial and temporal evolution of the surface temperature distribution. The equation to be solved is the heat conduction equation

$$\frac{\partial T(x,y,z,t)}{\partial t} = \left[K_x \frac{\partial^2 T(x,y,z,t)}{\partial x^2} + K_y \frac{\partial^2 T(x,y,z,t)}{\partial y^2} + K_z \frac{\partial^2 T(x,y,z,t)}{\partial z^2}\right], \quad (1)$$

where $T(x,y,z,t)$ is the temperature distribution, $K_i = \kappa_i/\rho c$ $(i = x,y,z)$ is the thermal diffusivity of the plate material, and κ, ρ, c are the thermal conductivity, density, and specific heat of the plate material, respectively.

With regard to the 3D non-linear computational complexity, the operation is often largely set by initial conditions and boundary conditions, so the initial conditions and the boundary conditions are optimized according to the real conditions. Especially the operation in real time by using the real time 3D irregular temperature data is also developed for the application. The preprocessing of the boundary conditions is proved to be reasonable by the numerical results.

The initial conditions for Eq. (1) are set as

$$T(x,y,z,t) = T_0(t=0). \tag{2}$$

The time interval of about 8 min between successive HL-2A discharges guarantees a uniform temperature distribution all over the plate at the beginning of each discharge. The boundary conditions for Eq. (1) are as follows.

(I) The time evolution of the two-dimensional temperature, measured by using an IR camera, is loaded onto the front-surface

$$T(x,y,z,t)|_{y=0} = T_0(x,z,t). \tag{3}$$

(II) The normal derivative $\partial T(x,y,z,t)/\partial y$ of the rear-surface temperature is assumed to be adiabatic under the up-surface and down-surface boundary conditions. This is equivalent to the assumption of negligible heat losses on the time scale of the discharge duration, i.e.,

$$P_d(t) = -\kappa \left.\frac{\partial T(x,y,z,t)}{\partial y}\right|_{y\to d} = 0, \tag{4}$$

where d is the divertor plate thickness.

(III) The boundary conditions of other surfaces are set to be radiative because the water-cooled system is not used

$$P(t) = \varepsilon\sigma[T(t)^4 - T_0^4], \tag{5}$$

where ε is the emissivity of surface, σ is the Stefan–Boltzmann constant, and T_0 is the temperature of the divertor structure in the calculation.

The plasma–material interaction occurs, of course, primarily in the front surface of the plate, so with these conditions, the time and space evolutions of deposited power density on the plate are calculated with the help of ANSYS

$$P(x,z,t) = -\left(\kappa_x \frac{\partial T(x,y,z,t)}{\partial x} + \kappa_y \frac{\partial T(x,y,z,t)}{\partial y} + \kappa_z \frac{\partial T(x,y,z,t)}{\partial z}\right)\Bigg|_{y=0}. \tag{6}$$

4. Model calculation and validation

In order to validate this analysis method, periodical heating pulses with a Gaussian space distribution and a maximum heat flux of 1 MW/m^2 are exerted on the surface as the input power, as shown in Fig. 3. For convenience, a local Cartesian coordinate is used in the simulation and also displayed in Fig. 3, and the y axis is perpendicular to the front surface pointing toward inside. The results calculated with ANSYS under the initial and the boundary conditions mentioned above are shown in Fig. 4. The front-surface temperature increases sharply due to the injection of heating power, and then decays after the heat flux has been switched off. While the rear-surface temperature grows slowly with increasing time (see Fig. 4(a)) and shows a delay due to the heat diffusion from the front surface to the rear surface. However, the slowly changing rear-surface temperature justifies the assumption of boundary condition (II) mentioned above. The comparison between the calculated heat flux and the applied heat flux shows little difference in spatial and temporal profile. These demonstrate that the 3D non-linear model is sufficiently reliable for the heat flux calculation.

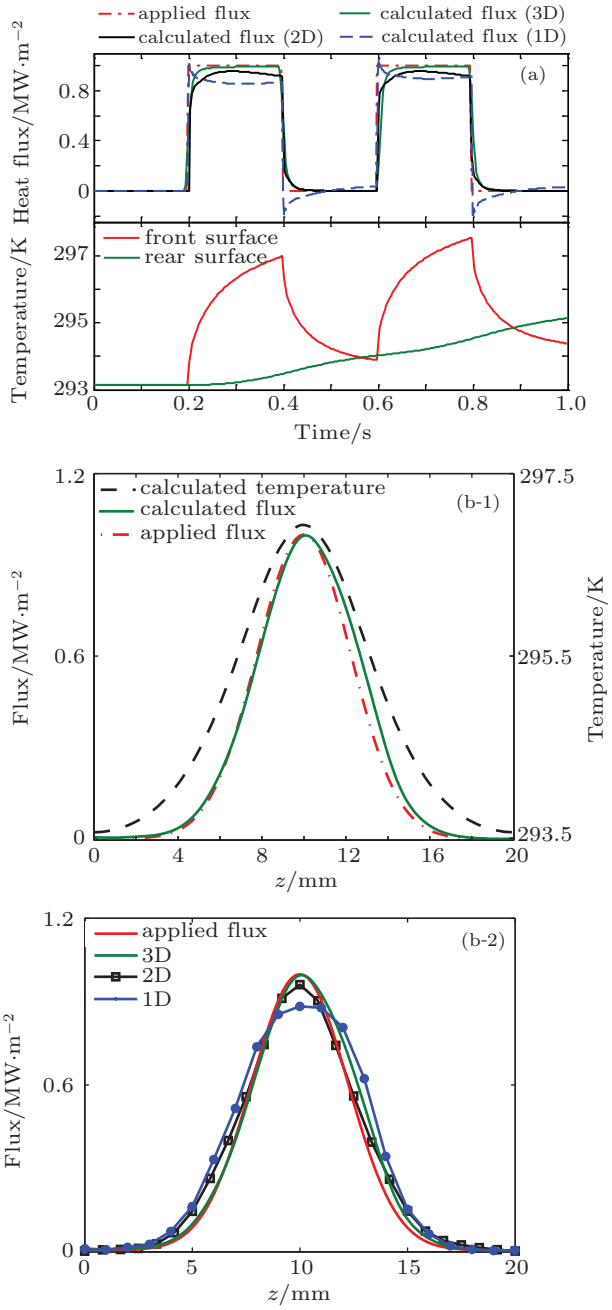

Fig. 4. (color online) (a) Time evolutions of input power, calculated temperature, and heat flux, and (b) profiles of input power, calculated temperature, and heat flux in the z direction. The time evolutions of heat flux and the profiles of heat flux in the z direction with 1D and 2D calculations are also presented.

For comparison, the heat flux profiles in the z direction and the time evolutions of heat flux with the 1D and 2D analyses are also shown in Fig. 4. A negative heat flux is shown in

the time evolution of heat flux with the 1D analysis. This behavior is accompanied by a sharp decrease in the injection heat flux. The surface temperature decays due to the heat diffusion into the plate after the heat flux has been switched off. The decay for a zero heat flux is fast, so a negative heat flux is needed to compensate the fast decay because the expected temperature value inside the plate is higher than the real temperature. For example, in the tail of the edge localized mode event (a heat flux burst), such a behavior has been reported from ASDEX upgrade IR measurements with 1D analysis.[9] In addition, the 1D and 2D analyses have broadened and flattened the peaked profiles because of neglecting heat propagation parallel to the surface. These behaviors, especially the broadened power deposition profiles, will result in inconsistency with the upstream power width and even overstating the cross-field heat conduction coefficient. However, compared with the results with 1D analysis, the profiles with 2D analysis are closer to those with 3D analysis. That is because in the 2D analysis, the heat conduction in the z direction is taken into account. Therefore, the comparison among heat flux profiles obtained with three different analysis methods demonstrates that the heat conduction dominates the process over the timescale of the diverted phase of a discharge, typically on the order of 1 s, and that it is necessary to take the 3D heat conduction into account for calculating the evolutions of heat flux on the divertor plates for the hot spot.

5. Application in experiment

Depending on the 3D analysis, the evolution of heat flux deposited on the outer divertor plate is obtained in a typical electron cyclotron resonant heating (ECRH) discharge as shown in Fig. 5. A temporal resolution of 16.7 ms is adopted in the IR camera measurement during this charge. The heat flux is about 0.5 MW/m^2 in ohmic heating phase and has a sharp increase up to about 1.3 MW/m^2 after 1 MW ECRH injection has been performed. It is consistent with the AXUV bolometer signal in the divertor chamber. This means that much more heat flows into the divertor during the ECRH phase. The deposited power density on the outer divertor plate in 820 ms is presented in Fig. 6(a), which illustrates an asymmetric distribution clearly. The width of density profile of power deposited along the torus is much narrower than that in the vertical direction. More details are given in Figs. 6(b) and 6(c). In the experimental results, the origin of Cartesian coordinate is translated to the mid-plane of the main chamber, but the coordinate directions are not changed, as shown in Fig. 2. That is why the z coordinate is negative in Figs. 6(a) and 6(b), but x- and y-coordinates are not changed. The FWHM of the profile in the z direction is about 25 mm for the ECRH phase, and it is about 3.8 mm in the x direction. The profile in the ohmic phase is very wide along the z direction compared with that in the ECRH phase, but does not show much difference in the x direction. And the profiles show typical asymmetrical distributions along the z direction, similar to the scenarios of other tokamaks.[1,4,9,12]. Moreover, at the boundaries both in the z and the x directions, the heat flux density is found to be approximately zero, that is why the heat conduction at the boundary can be assumed to be neglectable in the model (Section 3).

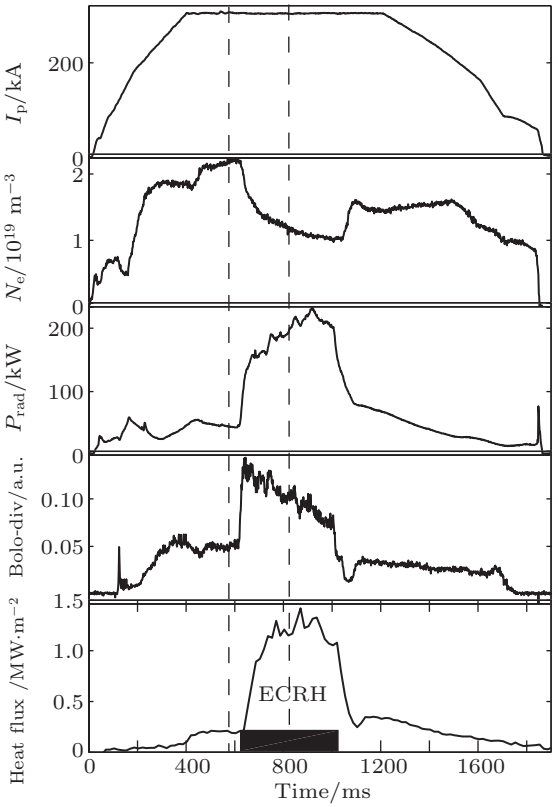

Fig. 5. Time evolutions of plasma current I_p, line averaged electron density N_e, plasma radiation P_{rad}, bolometer signal in divetor Bolo-div, and heat flux onto divertor target. The black rectangle represents the signal of ECRH. The vertical dash lines denote the times for the heat flux profiles shown in Fig. 6.

In addition, the normal 1D and 2D analysis results along the z direction are also given in Fig. 6(b) at the same time moment, i.e., 820 ms. It is clear that the peaks of power density are lower but the FWHMs are wider than those in the 3D case because the heat flow parallel to the surface is neglected in the 1D case and heat conducts along the torus in the 2D case. The FWHMs are about 40 mm for the 1D analysis and 30 mm for the 2D case, and are overestimated by 1.6 and 1.2 times, respectively. Subsequently, the heat flux peaks decrease from about 1.3 MW/m^2 to 1.18 MW/m^2 for the 1D case and 1.28 MW/m^2 for the 2D case.

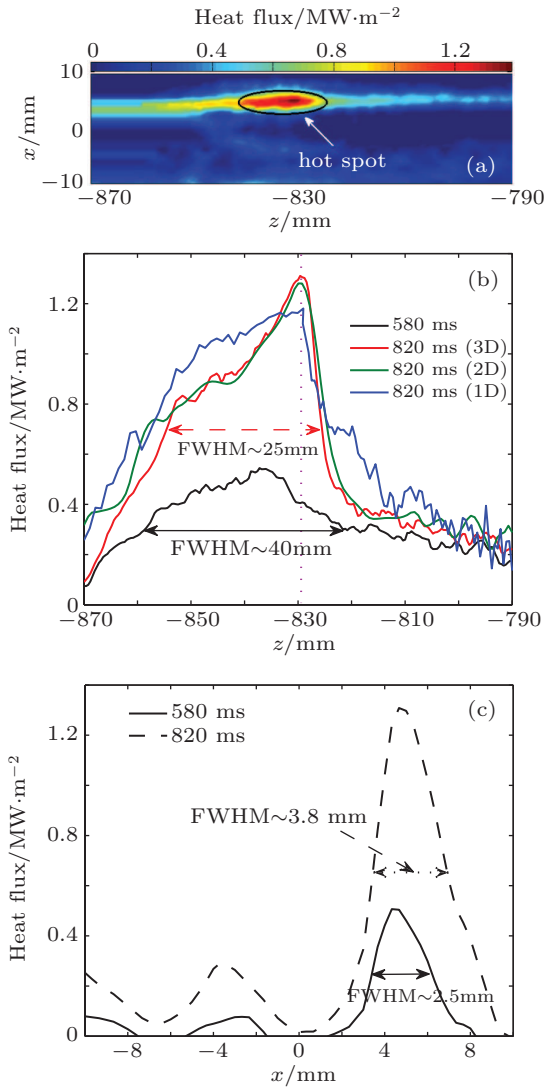

Fig. 6. (color online) (a) 2D image of power deposition at 820 ms, and power deposition profiles for various phases in (b) the z direction and (c) the x direction at the times corresponding to the vertical dash lines in Fig. 5. The profiles of heat flux in the z direction with 1D and 2D calculations are also shown.

6. Conclusions

The 3D model with real geometry and structure of the divertor plate on HL-2A is developed, based on which a 3D non-linear calculation is carried out. In this method, the heat conductance along the torus is taken into consideration, and the numerical simulations show its advantage of reconstructing the behaviors of power deposition profiles, especially for the heat flux bursts.

Therefore, this method is much beneficial for calculating the heat flux deposited on the divertor plate locally and providing the information about its spatial distribution characteristics. The heat power densities deposited on the outer divertor plate during the typical ohmic heating and ECRH phase are calculated from the IR camera diagnostics by using such a method. It is clear that the power deposited in the ohmic phase is about 0.5 MW/m^2, which is much lower than 1.3 MW/m^2 in the ECRH phase. And the FWHMs of the deposited power profiles in the z direction are about 40 mm for the ohmic phase and 25 mm for the ECRH phase. However, the FWHMs of the deposited power profiles in the x direction are much narrower than those in the z direction.

References

[1] Herrmann A, Junker W, Gunther K, Bosch S, Kaufmann M, Neuhauser J, Pautasso G, Richter T, Schneider R and ASDEX Upgrade Team 1995 *Plasma Phys. Control. Fusion* **37** 17

[2] Eich T, Herrmann A, Pautasso G, Andrew P, Asakura N, Boedo J A, Corre Y, Fenstermacher M E, Fuchs J C, Fundamenski W, Federici G, Gauthier E, Goncalves B, Gruber O, Kirk A, Leonard A W, Loarte A, Matthews G F, Neuhauser J, Pitts R A, Riccardo V and Silva C 2005 *J. Nucl. Mater.* **337–339** 669

[3] Eich T, Herrmann A, Neuhauser J and ASDEX Upgrade Team 2003 *Phys. Rev. Lett.* **91** 195003

[4] Eich T, Herrmann A, Neuhauser J, Dux R, Fuchs J C, Gunter S, Horton L D, Kallenbach A, Lang P T, Maggi C F, Maraschek M, Rohde V, Schneider W and ASDEX Upgrae Team 2005 *Plasma Phys. Control. Fusion* **47** 815

[5] Riccardo V, Andrew P, Ingesson L C and Maddaluno G 2002 *Plasma Phys. Control. Fusion* **44** 905

[6] C S Pitcher and P C Stangeby 1997 *Plasma Phys. Control. Fusion* **39** 779

[7] Eich T, Andrew P, Herrmann A, Fundamenski W, Loarte A, Pitts R A and JET-EFDA contributors 2007 Plasma Phys. Control. Fusion **49** 573

[8] Li Wei, Pan Y D, Yan L W, Yang Q W, Duan X R, Rao J, Feng B B, Lu J, Yi P and Ding X T 2007 *34th EPS Conf. on Plasma Physics*, July 2–6, 2007, Warsaw, Poland

[9] Herrmann A and ASDEX Upgrade team 2001 *28th EPS Conf. on Contr. Fusion and Plasma Phys.*, June 18–22, 2001, Funchal, Portugal

[10] Daviot R, Gauthier E, Carpentier S, Corre Y, Gardarein J L and JET EFDA Contributors 2009 *J. Nucl. Mater.* **390–391** 1070

[11] Gao J M, Liu Y, Li W, Cui Z Y, Zhou Y, Huang Y and Ji X Q 2010 *Chin. Phys.* B **19** 115201

[12] Petrie T W, Hill D N, Allen S L, Brooks N H, Buchenauer D A, Cuthbertson J W, Evans T E, Ghendrih P, Lasnier C J, Leonard A W, Maingi R, Porter G D, Whyte D G, Groebner R J, Jong R A, Mahdavi M A, Thompson S J, West W P and Wood R D 1997 *Nucl. Fusion* **37** 321